AD-A179 652 FORCED THREE DIMENSIONAL FLOW STRUCTURES(U) WEST VIRGINIA UNIV MORGANTOWN H VIETS SEP 85 AFOSR-TR-87-0392 AFOSR-82-0291 1/1

UNCLASSIFIED F/G 20/4 NL

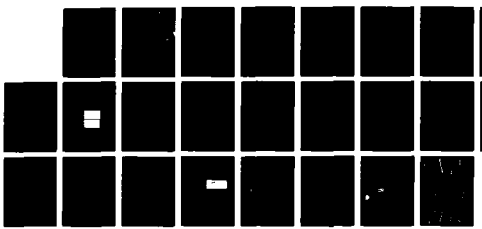

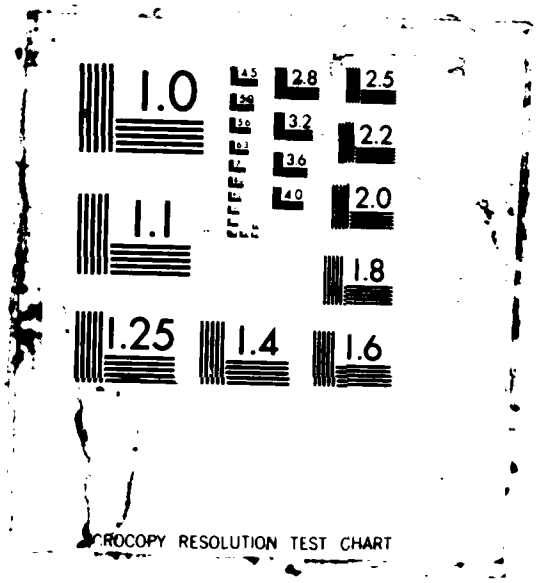
1.0
1.1
1.25
1.4
1.6
2.8
3.2
3.6
4.0
2.5
2.2
2.0
1.8
CROCOPY RESOLUTION TEST CHART

SECUR

AD-A179 652

DTIC FILE COPY (2)

T DOCUMENTATION PAGE

1a. REPORT SECURITY CLASSIFICATION UNCLASSIFIED	1b. RESTRICTIVE MARKINGS
2a. SECURITY CLASSIFICATION AUTHORITY	3. DISTRIBUTION/AVAILABILITY OF REPORT APPROVED FOR PUBLIC RELEASE DISTRIBUTION IS UNLIMITED
2b. DECLASSIFICATION/DOWNGRADING SCHEDULE	
4. PERFORMING ORGANIZATION REPORT NUMBER(S)	5. MONITORING ORGANIZATION REPORT NUMBER(S) AFOSR-TR- 87-0392
6a. NAME OF PERFORMING ORGANIZATION UNIVERSITY OF WEST VIRGINIA 6b. OFFICE SYMBOL (If applicable)	7a. NAME OF MONITORING ORGANIZATION AFOSR/NA
6c. ADDRESS (City, State and ZIP Code) MORGANTOWN, WEST VIRGINIA 26506	7b. ADDRESS (City, State and ZIP Code) BUILDING 410 BOLLING AFB, DC 20332-6448
8a. NAME OF FUNDING/SPONSORING ORGANIZATION AFOSR/NA 8b. OFFICE SYMBOL (If applicable) NA	9. PROCUREMENT INSTRUMENT IDENTIFICATION NUMBER AFOSR 82-0291
8c. ADDRESS (City, State and ZIP Code) BUILDING 410 BOLLING AFB, DC 20332-6448	10. SOURCE OF FUNDING NOS PROGRAM ELEMENT NO: 61102F PROJECT NO.: 2307 TASK NO.: A2 WORK UNIT NO.
11. TITLE (Include Security Classification) (U) FORCED THREE DIMENSIONAL FLOW STRUCTURES	
12. PERSONAL AUTHOR(S) H. VIETS	
13a. TYPE OF REPORT FINAL	13b. TIME COVERED FROM _____ TO _____
14. DATE OF REPORT (Yr., Mo., Day) SEPT 1985.	15. PAGE COUNT 35
16. SUPPLEMENTARY NOTATION	

DTIC ELECTE APR 2 7 1987 S E

17 COSATI CODES		
FIELD	GROUP	SUB GR

18 SUBJECT TERMS (Continue on reverse if necessary and identify by block number)
UNSTEADY FLOW, SEPARATED FLOW, VORTEX.

19. ABSTRACT (Continue on reverse if necessary and identify by block number)

Forced unsteadiness in a two-dimensional jet using fluidically imposed excitation in the jet nozzle has been studied experimentally. A second method of introducing unsteadiness using a rotating cam-shaped rotor has also been studied in the jet flow as well as in flows over rearward facing ramps and backsteps. Results show that the separation and reattachment conditions can be controlled in this manner and that jet and wake spreading characteristics can be modified using these techniques. Two techniques for identification of rotational vortex structures have been developed. Ther first uses phase information in the discrete Fourier treansform of the field while the second involves spatial behavior of local orthogonal decomposition components.

20. DISTRIBUTION/AVAILABILITY OF ABSTRACT UNCLASSIFIED/UNLIMITED ☒ SAME AS RPT ☐ DTIC USERS ☐	21 ABSTRACT SECURITY CLASSIFICATION UNCLASSIFIED
22a. NAME OF RESPONSIBLE INDIVIDUAL James McMichael	22b. TELEPHONE NUMBER (Include Area Code) 202 [illegible]
	22c. OFFICE SYMBOL NA

DD FORM 1473, 83 APR EDITION OF 1 JAN 73 IS OBSOLETE

UNCLASSIFIED

FORCED THREE DIMENSIONAL FLOW STRUCTURES

Final Report
AFOSR Grant No. 82-0291

Prepared by
Herman Viets, Principal Investigator
West Virginia University
Morgantown, West Virginia

September 1985

ORTHOGONAL DECOMPOSITION OF FLOW FIELDS IN DISTANCE/DISTANCE/TIME SPACE

INTRODUCTION

Bethke and Viets have developed two techniques for identification of rotational structures (vortices) in flow fields.[1,2] The first utilizes phase information in the discrete Fourier transform of the field while the second involves spatial behavior of local orthogonal decomposition components of the field. While the second method is generally superior to the first, both methods required whole field input data at a given instant in time. This research addresses the relaxation of this restriction through the analysis of local field behavior as a function of time, and is based on the second method.

ORTHOGONAL DECOMPOSITION IN THE DISTANCE/DISTANCE/TIME DOMAIN

As an approach to distance/distance/time (d/d/t) orthogonal decomposition, suppose we consider flow velocities taken at 4 fixed rectangularly related locations at two different times. These are depicted in Figure 1 as velocities 1-4 at one sample time say k-1, and velocities 5-8 at the next sample time, k. The d/d/t data cell contains 8 "locations" each having a u and v spatial velocity component. Thus at any two adjacent sample times we have a data cell with 16 velocities, u_1, v_1, through u_8, v_8. The approach adopted here will model the behavior of the flow in a spatially fixed data cell and then study the cell behavior as a function of time to extract flow field information.

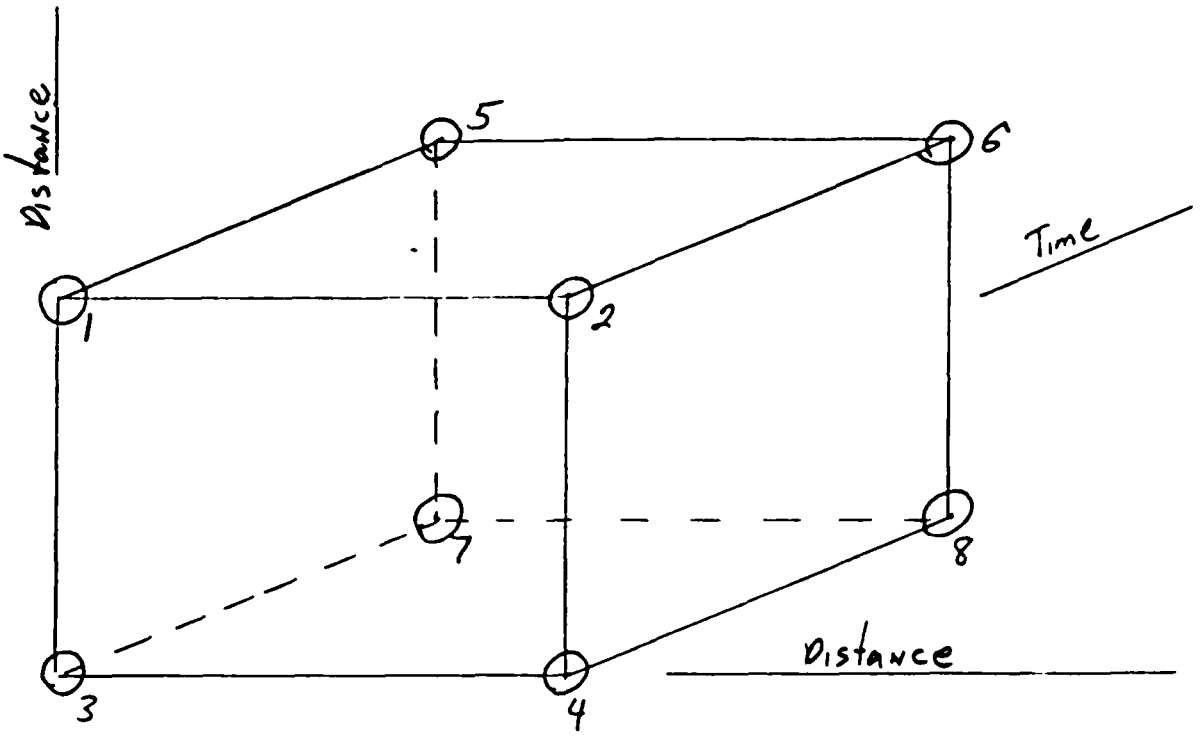

Figure 1. Distance/Distance/Time Flow Data Cell

The data in a d/d/t flow cell will be modeled with 12 independent measures of its behavior. These 12 descriptors (α's) will describe the local time behavior of six spatial flow measures (β's) at the two different cell times (k and k-1). A set of six β's describe the amount of rotation, horizontal and vertical translation, horizontal and vertical expansion, and shear at each sample time. That is at a given sample time, say k-1, the velocities $u_1, v_1, u_2, v_2, u_3, v_3, u_4, v_4$ will be described by a β weighted set of basis vectors plus an error vector (ϵ's), i.e.

$$\begin{bmatrix} u_1 \\ v_1 \\ u_2 \\ v_2 \\ u_3 \\ v_3 \\ u_4 \\ v_4 \end{bmatrix} = \begin{bmatrix} -A & 1 & 0 & -1 & 0 & B \\ -B & 0 & 1 & 0 & 1 & -A \\ -A & 1 & 0 & 1 & 0 & B \\ B & 0 & 1 & 0 & 1 & A \\ A & 1 & 0 & -1 & 0 & -B \\ -B & 0 & 1 & 0 & -1 & -A \\ A & 1 & 0 & 1 & 0 & -B \\ B & 0 & 1 & 0 & -1 & A \end{bmatrix} \begin{bmatrix} \beta_1 \\ \beta_2 \\ \beta_3 \\ \beta_4 \\ \beta_5 \\ \beta_6 \end{bmatrix} + \begin{bmatrix} \epsilon_1 \\ \epsilon_2 \\ \epsilon_3 \\ \epsilon_4 \\ \epsilon_5 \\ \epsilon_6 \\ \epsilon_7 \\ \epsilon_8 \end{bmatrix}$$

It is seen that the β basis vectors describe the six flow types shown in Figure 2, where A and B are the vertical and horizontal dimension of the data cell.

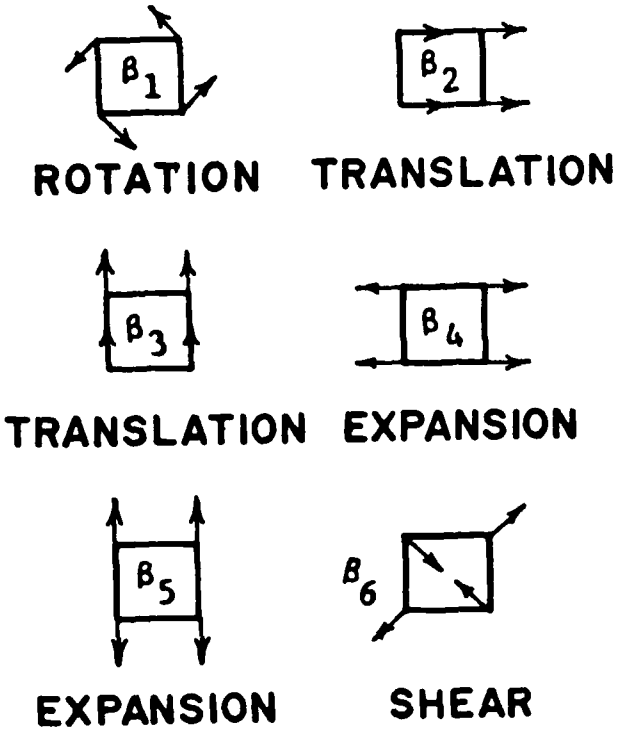

Figure 2 β Basis Vector Components

The data in a d/d/t flow cell will be modeled by least squares fitting the 6 orthogonal descriptors, β's, at each of the two sample times. At sample time k-1 this will give $\beta_1(k-1),\ldots,\beta_6(k-1)$ and at sample time k, $\beta_1(k),\ldots,\beta_6(k)$. Time will be incorporated via the sum, $\alpha_{is}(k)$, and difference, $\alpha_{id}(k)$, of the β types. That is,

$$\alpha_{is}(k) = \frac{1}{2}\left[\beta_i(k) + \beta_i(k-1)\right]$$

and

$$\alpha_{id}(k) = \frac{1}{2}\left[\beta_i(k) - \beta_i(k-1)\right].$$

Thus each distance/distance/time data cell will be described by the 12 α parameters $\alpha_{1s},\ldots,\alpha_{6s},\alpha_{1d},\ldots,\alpha_{6d}$.

The modeling process described above can be viwed as a linear least squares operation in which the vector composed of the 16 velocities of a d/d/t data cell, $u_1,v_1,\ldots u_8,v_8$, is to be modeled as an α weighted combination of 12 basis vectors plus an vector of errors, ϵ. That is,

$$
\begin{bmatrix} u_1 \\ v_1 \\ u_2 \\ v_2 \\ u_3 \\ v_3 \\ u_4 \\ v_4 \\ u_5 \\ v_5 \\ u_6 \\ v_6 \\ u_7 \\ v_7 \\ u_8 \\ v_8 \end{bmatrix}
=
\underbrace{\begin{bmatrix}
-A & 1 & 0 & -1 & 0 & B & +A & -1 & 0 & +1 & 0 & -B \\
-B & 0 & 1 & 0 & 1 & -A & +B & 0 & -1 & 0 & -1 & +A \\
-A & 1 & 0 & 1 & 0 & B & +A & -1 & 0 & -1 & 0 & -B \\
B & 0 & 1 & 0 & 1 & A & -B & 0 & -1 & 0 & -1 & -A \\
A & 1 & 0 & -1 & 0 & -B & -A & -1 & 0 & +1 & 0 & +B \\
-B & 0 & 1 & 0 & -1 & -A & +B & 0 & -1 & 0 & +1 & +A \\
A & 1 & 0 & 1 & 0 & -B & -A & -1 & 0 & -1 & 0 & +B \\
B & 0 & 1 & 0 & -1 & A & -B & 0 & -1 & 0 & +1 & -A \\
-A & 1 & 0 & -1 & 0 & B & -A & 1 & 0 & -1 & 0 & B \\
-B & 0 & 1 & 0 & 1 & -A & -B & 0 & 1 & 0 & 1 & -A \\
-A & 1 & 0 & 1 & 0 & B & -A & 1 & 0 & 1 & 0 & B \\
B & 0 & 1 & 0 & 1 & A & B & 0 & 1 & 0 & 1 & A \\
A & 1 & 0 & -1 & 0 & -B & A & 1 & 0 & -1 & 0 & -B \\
-B & 0 & 1 & 0 & -1 & -A & -B & 0 & 1 & 0 & -1 & -A \\
A & 1 & 0 & 1 & 0 & -B & A & 1 & 0 & 1 & 0 & -B \\
B & 0 & 1 & 0 & -1 & A & B & 0 & 1 & 0 & -1 & A
\end{bmatrix}}_{\text{Sum basis vectors}\quad\quad\text{diff. basis vectors}}
\begin{bmatrix} \alpha_{1s} \\ \alpha_{2s} \\ \alpha_{3s} \\ \alpha_{4s} \\ \alpha_{5s} \\ \alpha_{6s} \\ \alpha_{1d} \\ \alpha_{2d} \\ \alpha_{3d} \\ \alpha_{4d} \\ \alpha_{5d} \\ \alpha_{6d} \end{bmatrix}
+
\begin{bmatrix} \epsilon_1 \\ \epsilon_2 \\ \epsilon_3 \\ \epsilon_4 \\ \epsilon_5 \\ \epsilon_6 \\ \epsilon_7 \\ \epsilon_8 \\ \epsilon_9 \\ \epsilon_{10} \\ \epsilon_{11} \\ \epsilon_{12} \\ \epsilon_{13} \\ \epsilon_{14} \\ \epsilon_{15} \\ \epsilon_{16} \end{bmatrix}
$$

sample time k-1

sample time k

or in matrix notation

$$\bar{V} = X\,\bar{\alpha} + \bar{\epsilon}$$

Note that the 1st and 7th basis vectors correspond to the time sum and difference of spatial rotation respectively, the 2nd and 8th vectors the time sum and difference of spatial horizontal translation, and so forth. Also note that the basis vectors are all mutually orthogonal which not only greatly simplifies least squares estimation of the α values but makes these estimates statistically independent.

Least squares estimates of the α values, $\hat{\alpha}$, are readily found using

$$\hat{\bar{\alpha}} = [X^T X]^{-1} X^T \bar{V} = \frac{1}{8} X^T \bar{V}$$

where $A^2+B^2 = 1$.

PROPERTIES OF THE TIME DOMAIN SUM AND DIFFERENCE

As noted above, this research is based on time domain behavior of a given orthogonal flow discriptor, (β_i), as exemplified by the sum and difference of this discription at adjacent sample times. That is, for the ith orthogonal descriptor β_i the sum descriptor, α_{is} at sample times k and k-1, is

$$\alpha_{is}(k) = \frac{1}{2}(\beta_i(k) + \beta_i(k-1))$$

or more conviently (i understood)

$$\alpha_s(k) = \frac{1}{2}(\beta(k) + \beta(k-1)).$$

The difference descriptor is thus written as

$$\alpha_d(k) = \frac{1}{2}(\beta(k) - \beta(k-1)).$$

These sum and difference operations can be viewed as time domain digital filtering of the β vlaues to produce the α values as depicted in Figure 3.

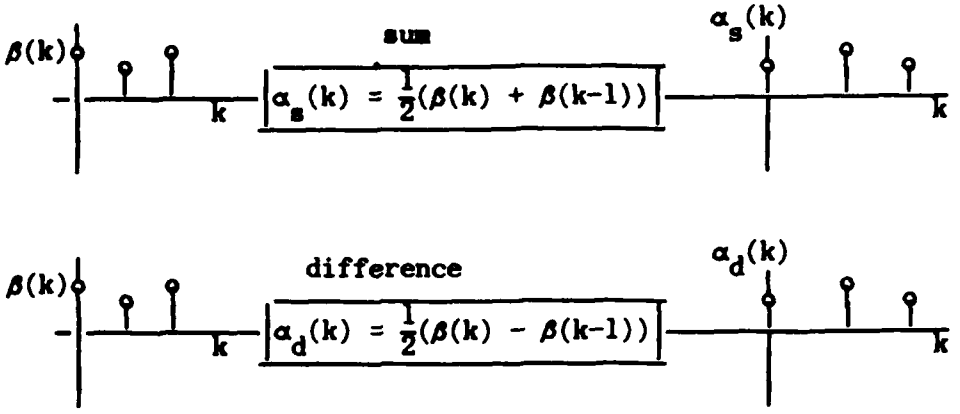

Figure 3. Time domain filtering operations

Insight into the sum and difference operations can be gained through their frequency response. For example, if we take the Z-transform of the sum operation

$$\alpha_s(K) = \frac{1}{2}(\beta(K) + \beta(K-1))$$

we get

$$\alpha_s(Z) = \frac{1}{2}(\beta(Z) + Z^{-1}\beta(Z)).$$

The ratio of the output and input produces the transfer function, $H_s(Z)$, of this filtering operation

$$H_s(Z) \equiv \frac{\alpha_s(Z)}{\beta(Z)} = \frac{1}{2}(1+Z^{-1}) = \frac{\frac{1}{2}(Z+1)}{Z} .$$

Setting the complex variable Z equal to $e^{j\omega T}$, where T is the time between samples we get the frequency response of the filtering operation, i.e.

$$H_s(e^{j\omega T}) = \frac{\frac{1}{2}(e^{j\omega T}+1)}{e^{j\omega T}}$$

$$= \frac{\frac{1}{2}\, e^{j\omega T/2}[e^{j\omega T/2} + e^{-j\omega T/2}]}{e^{j\omega T}}$$

$$= e^{-j\omega T/2} \cos(\omega T/2)$$

The difference operation likewise has the transfer function

$$H_d(Z) = \frac{\frac{1}{2}(Z-1)}{Z}$$

and the frequency responce

$$H_d(e^{j\omega T}) = e^{-j(\omega T/2-\pi)} \sin(\omega T/2).$$

The frequency response magnitudes for the sum and difference oeprations are shown in Figure 4.

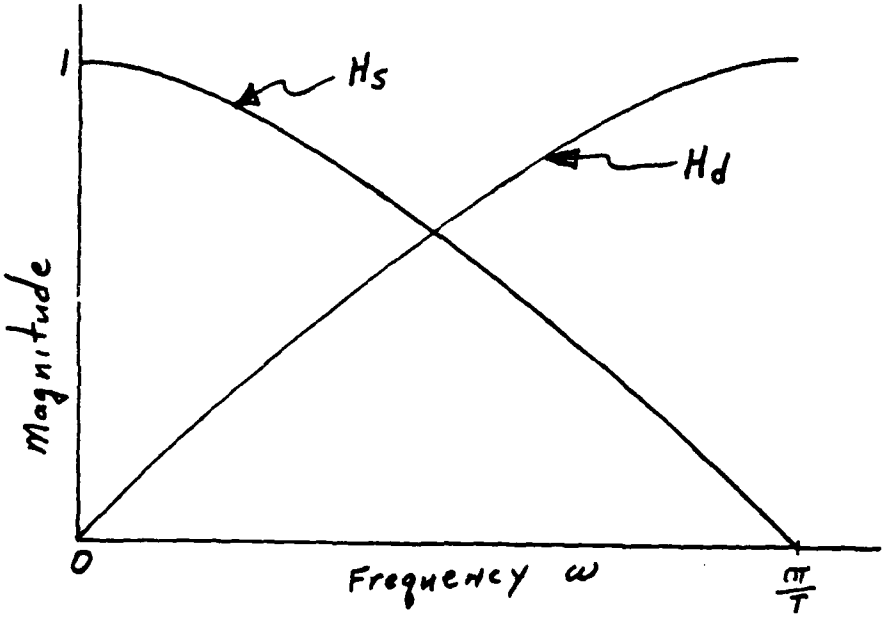

Figure 4. Frequency Response Magnitudes

It is seen that the sum and difference are low and high pass filter operations with gains of $\cos(\omega T/2)$ and $\sin(\omega T/2)$ respectively. That is, the sum operation enhances the low while suppressing the high frequency temporal behavior of a given β_i flow descriptor. The difference operation does just the opposite, suppressing low and enhancing high temporal frequencies. It should be noted that "low" and "high" frequencies here are relative to one

half the sample frequency, the highest unaliased frequency in the data, π/T radians/second.

The sum and difference operations are also related to the discrete Fourier Transform (DFT) which transforms N discrete time data values to N discrete frequency (spectral) values via the operation

$$F(\ell\Omega) = \sum_{K=0}^{N-1} f(KT)e^{-jkT\ell\Omega}$$

where

$$\Omega = \frac{2\pi}{NT} .$$

For the two point case (N=2) this becomes

$$F(0\Omega) = f(0T) + f(1T)$$

and

$$F(1\Omega) = f(0T) - f(1T) \quad .$$

which is proportional to the previously discussed sum and difference operations but with the terms reversed in the difference. Repetative use of sum and difference to describe temporal behavior of a given flow parameter, β_i, can thus be considered as akin to repetitively computing its 2-point frequency spectrum as a function of time.

SYNTHETIC VORTEX TEST RESULTS

The synthetic, counter clockwise velocity field shown in Figure 5 was used to test the orthogonal decomposition method. The field was assumed to be moving to the right at a constant velocity with unchanging rotational behavior. The distance/distance/time data cells were formed using the velocities at 4 rectangularly adjacent locations to respresent a sample time, say k-1, and the 4 location velocities immediately to the left as time k.

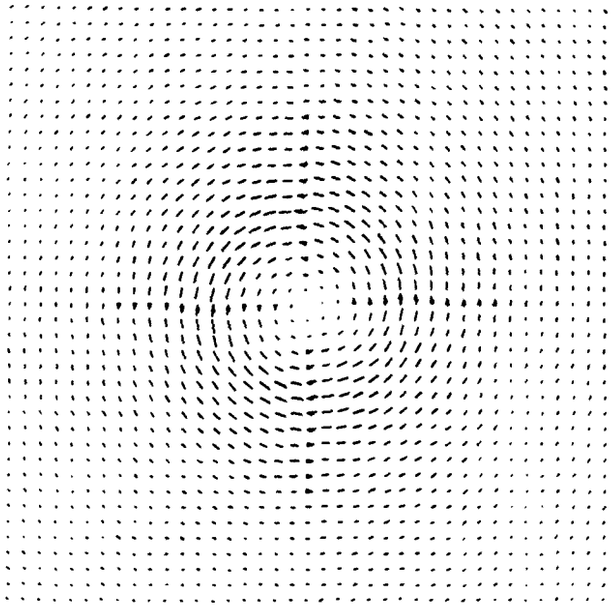

Figure 5. Velocity distribution in the synthetic vortex.

Each of the 12 α parameters was computed for each of the d/d/t data cells, so constructed, in the field.

The synthetic field results are displayed in a set of 6 vector field plots, one plot for each flow descriptor (β) type; rotation, horizontal translation, and so forth. Each vector in a given plot is formed by the sum and difference, α_s and α_d, values of a d/d/t data cell. The sum, α_s, and the difference, α_d, being the horizontal and vertical vector component lengths respectively. The origin of each vector is determined vertically by the vertical location of the data cell in the flow field and horizontally by the data cell sample time, k. To readily allow comparison with smoke pictures and other instantaneous time field descriptions, the earliest time data is on the right of the plots, with time increasing to the left.

These plots exhibit the behavior one would see monitoring the velocities at 4 rectangularly oriented locations as a funciton of the flow descriptor type (β plot type), vertical cell location (plot row), and time (location within the plot row); as exhibited by the α vectors.

The synthetic vortex β_1 plot (rotation), Figure 6, shows vortex activity along a given row as viewed right to left (increasing time). That is, the horizontal length of the vector grows and subsides indicating vortex strength, and the vertical length goes positive and then negative indicating increasing and then decreasing vorticity as the vortex passes. The time trajectory of the vector along a given row thus indicates the presence and rate of change of the vorticity at that vertical location in the flow field. The characteristic vector time trajectories for rows above and below the vortex center are displayed on the plot for this counter clockwise example. A like field,

rotating clockwise, would cause the horizontal vector components ~~displayed here~~ to be of opposite sign at all times and would result in the dashed trajectories.

The β_1 (rotation) plot clearly indicates the presence of vorticity that is, having vectors of significant non-zero length. The horizontal center of the vortex is indicated by a horizontal β_1 vecotr, i.e., one with vorticity but of unchanging strength. The vertical center of the vortex, however, is difficult to locate using only one vector row (set of 4 sensors) because each row has a similar vector trajectory. Observation of the β_1(rotation) vector thus indicates the presence of vorticity and the streamwise location of the vortex center but not the anti-streamwise center location.

Figure 7, the β_2 horizontal translation plot, provides information not present in the Figure 6 rotation plot. The vector trajectoris are all clockwise (c.w.) but the sum (horizontal) vector component (α_s) are negative above the vortex center and positive below. A singlerow in Figures 6 and 7 can thus locate the vortex center in time and indicate if the rotational center is above or below the observation row. Figure 8, the β_3 vertical translation plot, again shows c.w. vector trajectories but in this case the trajectories go both positive and negative in the horizontal direction. These trajectories are of similar nature above and below the vortex center, and are thus of use in detecting vorticity, its rotational direction, and locating it in time, but not in the antistreamwise direction.

Figures 9 and 10, horizontal and vertical expansion, each show different patterns above and below the center streamline, allowing the vortex center to be so identified as well as in time. Rotation direction is also evident.

Figure 11, shear, produces unique double rotation trajectories suitable for identification of the vortex center in the streamwise but not the

antistreamwise directions. The c.w. trajectories indicate c.c.w. vortex rotation.

D/D/T DECOMPOSITION OF AN ACTUAL FLOW FIELD

The analysis and display techniques applied to the synthetic flow field were applied to the field shown in Figure 12. This field was generated by a cam shaped rotor, rotating at the wall of a low speed wind tunnel.

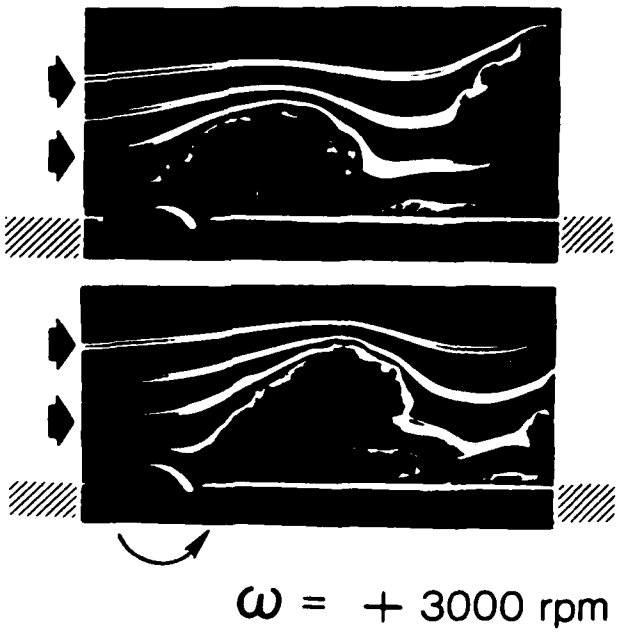

Figure 12. Smoke flow visualization of the rotor flowfield.

A set of instantaneous flow field velocities from the tunnel are shown in Figure 13.

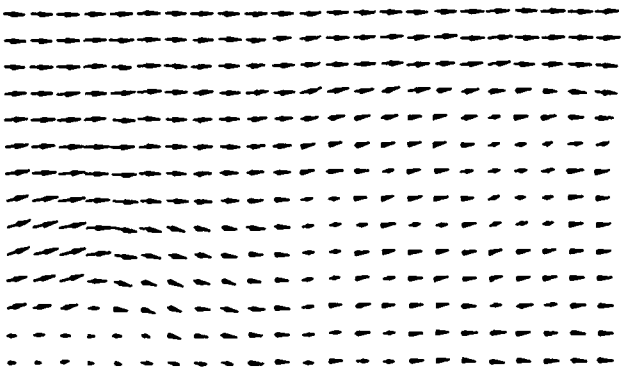

Figure 13 Instantaneous flowfield velocities

The instantaneous velocity field shown in Figure 13 was analyzed as time invariant translational data using the same techniques as above. Figure 14 displays the rotational (β_1) behavior. The clockwise (c.w.) vortices in the lower left and upper right are clearly apparent as indicated by the large horizontal vector components pointing to the left. A small c.c.w vortex is also noted at the lower center of the field as indicated by short vectors to the right. It is seen that any one row of data, 4 senor locations as a function of time, provides vorticity information along that row as well as the streamwise locations of the vortex centers. In addition it is seen that vector behaviors along rows in or near vortex centers exhibit strong smooth behaviors while those along the vortex edge exhibit more erratic, high frequency movements.

Figure 15 shows the time behavior of the horizontal translation component of the field. It is seen that all vecotrs in the field have a positive bias direction indicating general field flow to the right. Vortex activity along a row is therefore best indicated by the vertical activity of these vectors. In the rows below a c.w. vortex center the vectors nod down and then up with time. In the rows above they go up and then down. Given the fact these vortices are c.w. (from Figure 14) this information not only indicates the streamwise location of the vortices but also if they are above or below the observed row. It is also interesting to note that the vectors in this field seem to generally depict the trajectory of the vortex center. Figure 16 shows the time activity of the vertical translation activity parameter β_3. As expected, vortex activity is indicated by strong sweeping movements along a given row. The streamwise location of the vortex being indicated being vertical down vector (c.c.w) or vertical up vector (c.w.) It is noted that along any row the vectors rotate approximately the same amount, (one revolution c.w. independent of the row).

Figures 17 and 18 show the cell horizontal and vertical expansion time activity along a row (time, as usual, increasing right to left). Comparison of these figures with their synthetic vortex counterparts, Figures 9 and 10, once again indicates the existance of and streamwise location of the vortex, its rotation direction, and if the vortex center is below or above the observed row.

Figure 19 shows the row time behavior of the shear parameter, β_6. The characteristic double oscillation behavior shown in the synthetic case is

again seen. As before, the regions of vorticity are marked by significant activity in the time behavior of this vector.

CONCLUSION

This study explores the utility of locating rotational structures in a flow field by locally decomposing the fields spatial and time behavior via a set of orthogonal descriptors and then viewing these descriptions as a function of time. It is seen that these descriptions, based on a 8 point distance/distance/time cell, can identify rotational structures, their direction of rotation, their streamwise location, and if they are above or below the streamwise observation location.

The behavior of the cell parameters, as a function of time (streamwise) and antistreamwise displacement, was very distinct and clearly exhibited a great deal of structure in addition to those aspects discussed above. It is reasonable that the method of flow decomposition and display presented here may offer additional insights into observed flow fields dynamics.

Further investigation might be conducted via the four lcoation two sample time cell, as above, or perhaps by a two location four sample time configuration. In either case the time behavior of the computed vectors might well be displayed, recorded and studied via a storage osillosope.

Fig 6

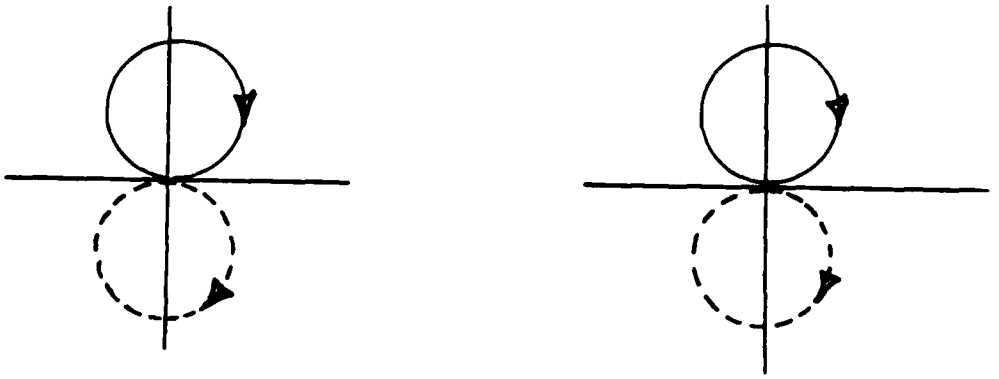

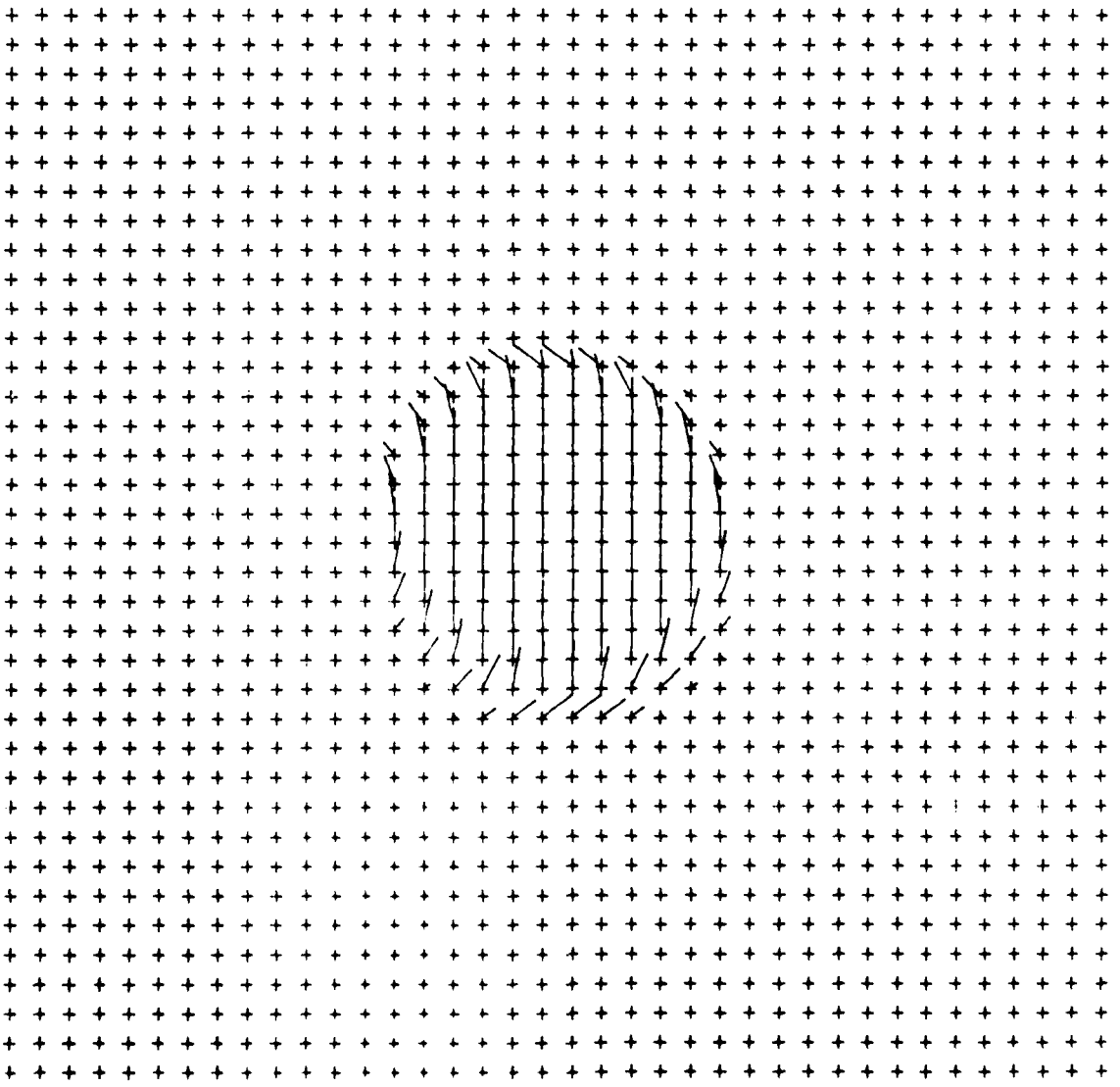

K=1

Fig 7

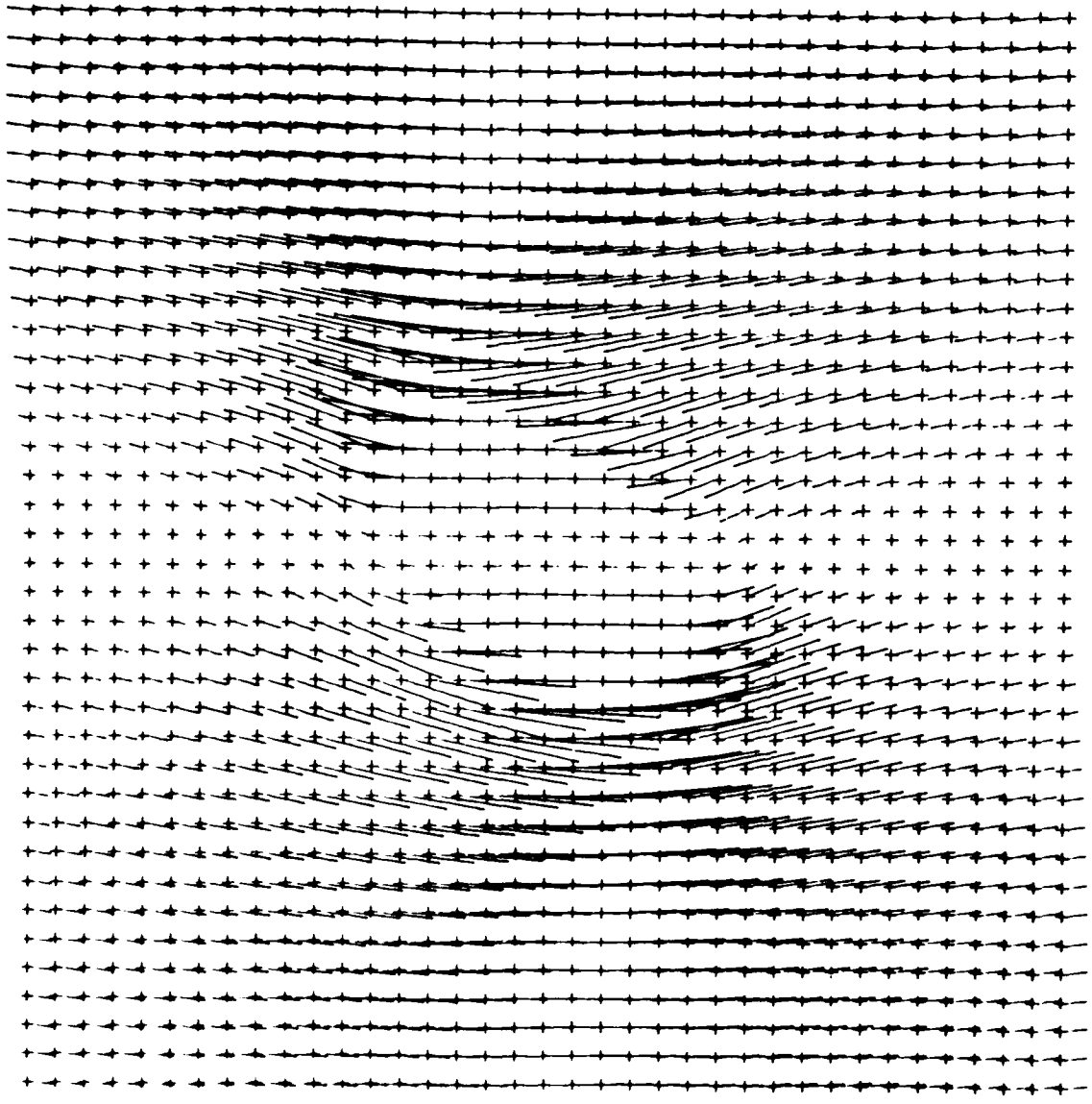

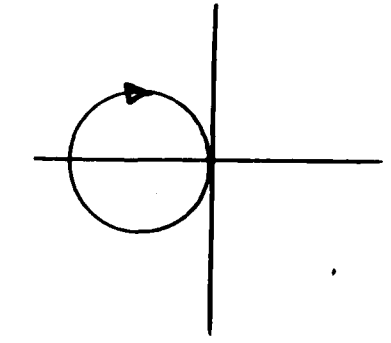

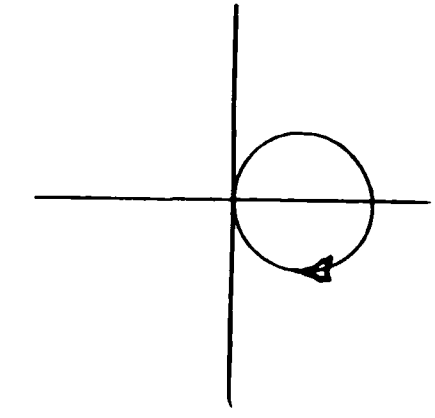

$\lambda = 3$

Fig 8

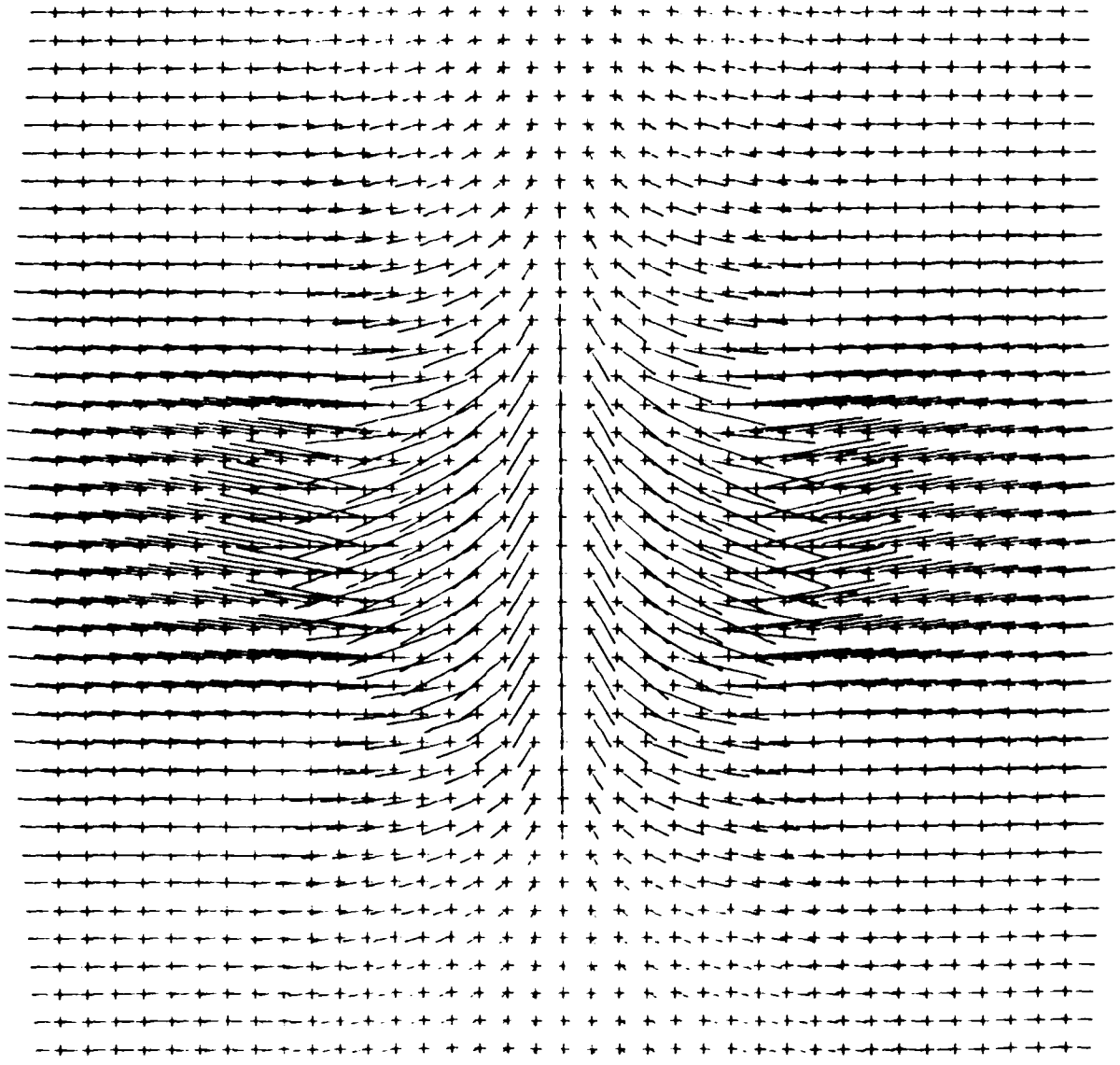

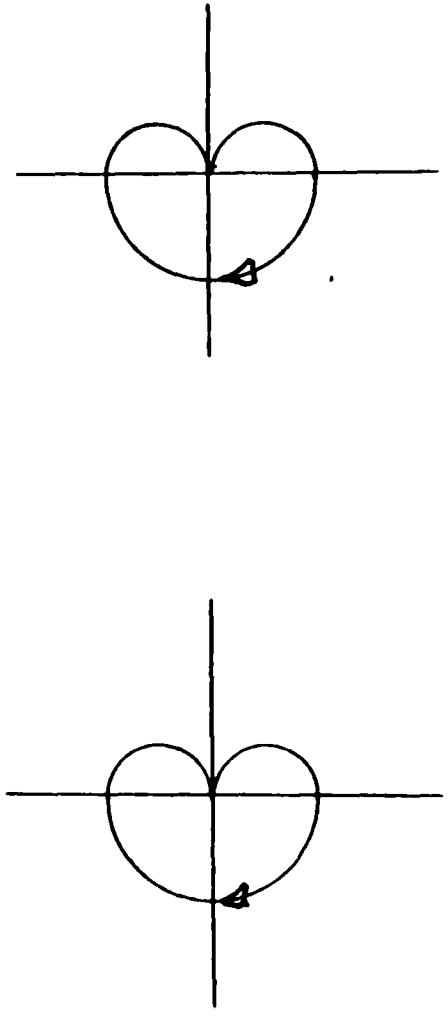

Fig 9

Fig 10

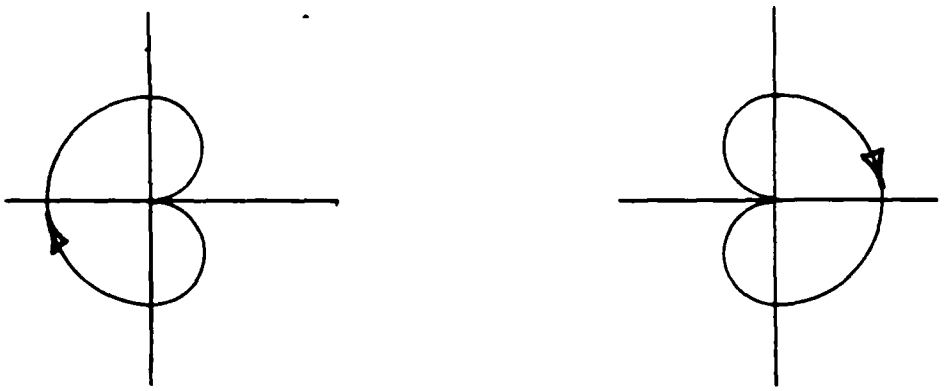

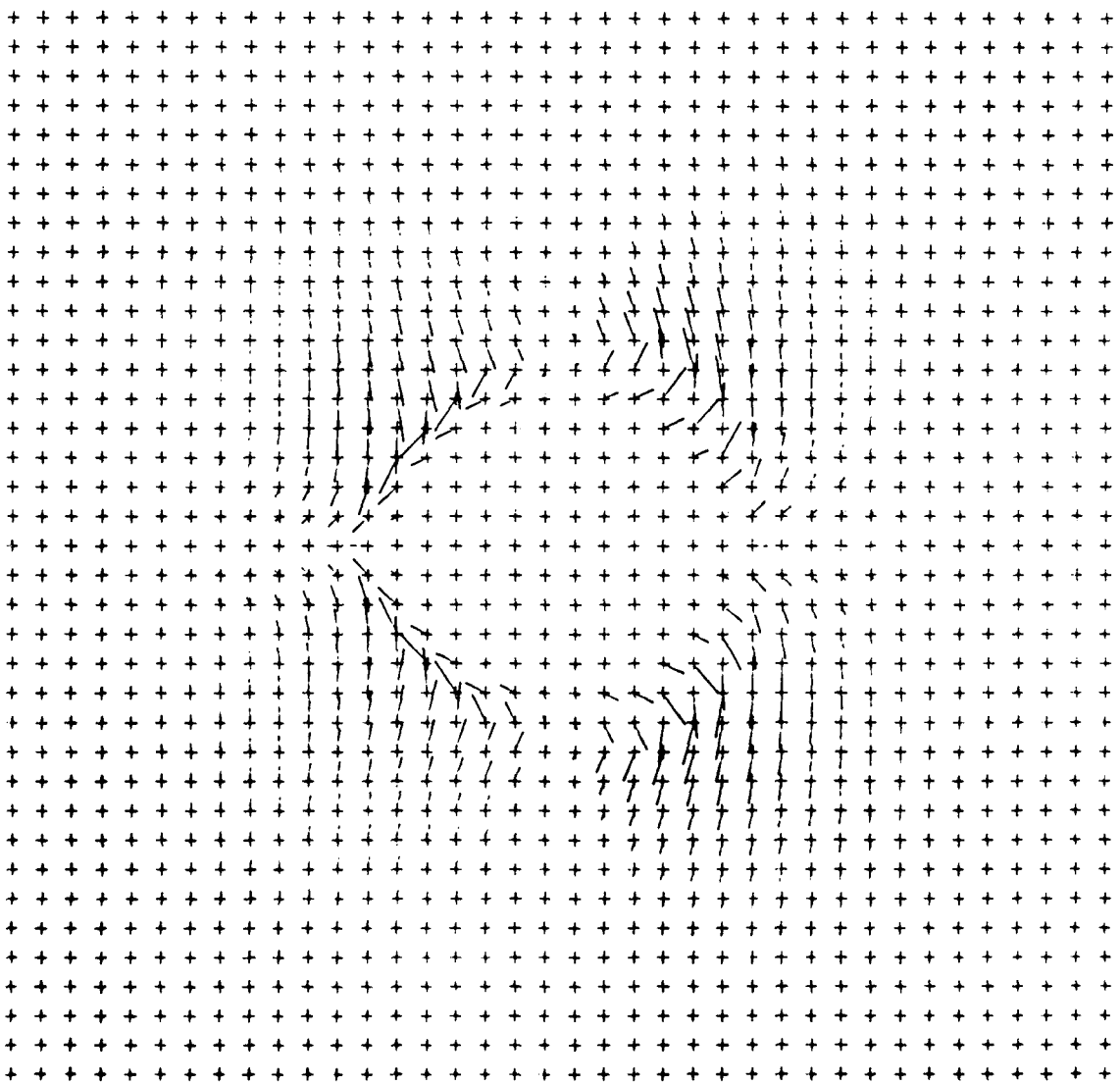

Fig 11

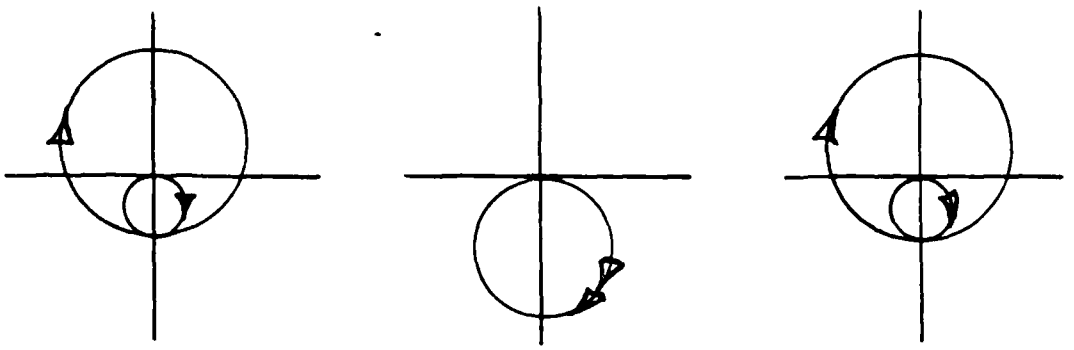

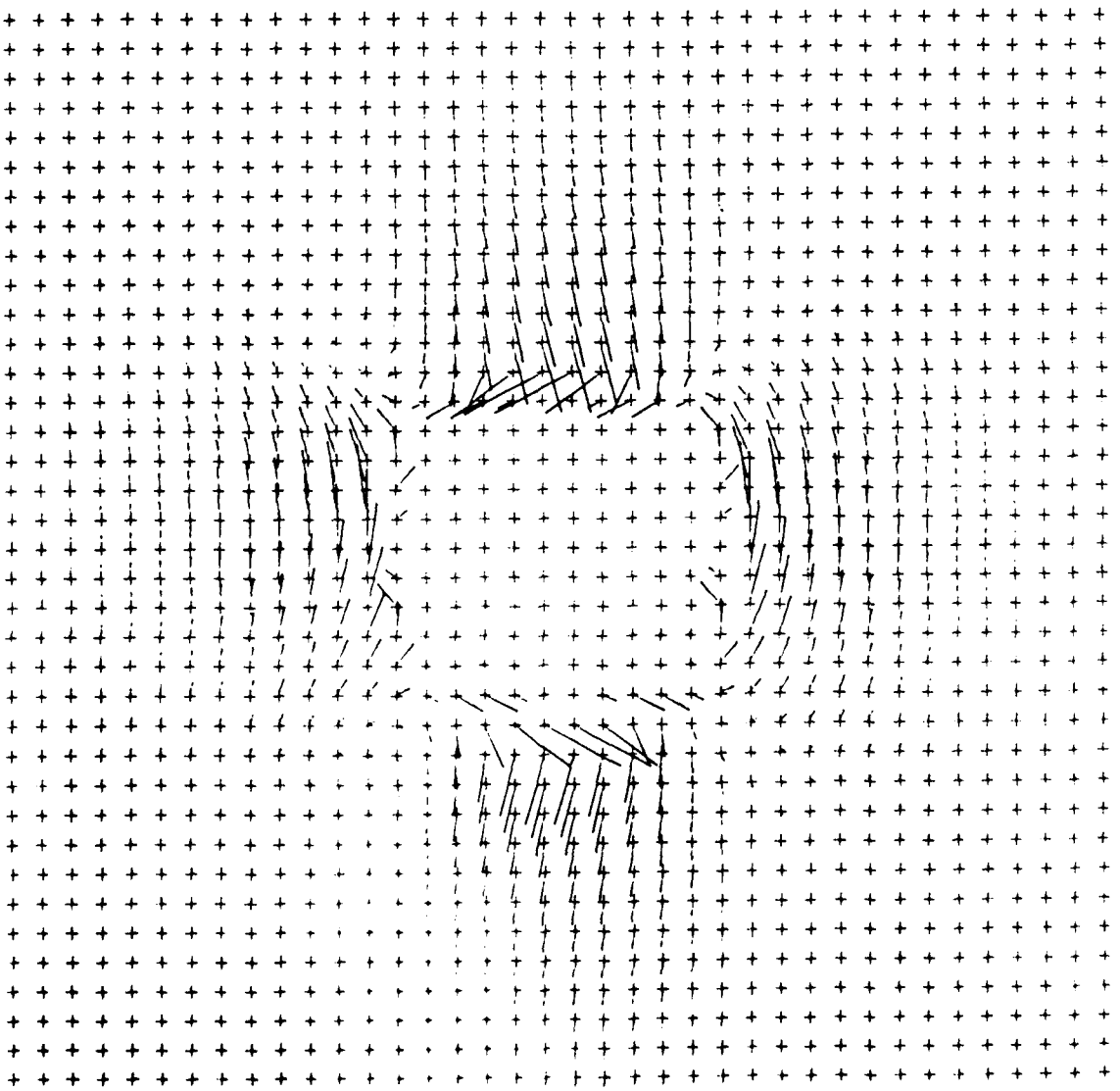

Fig. 14

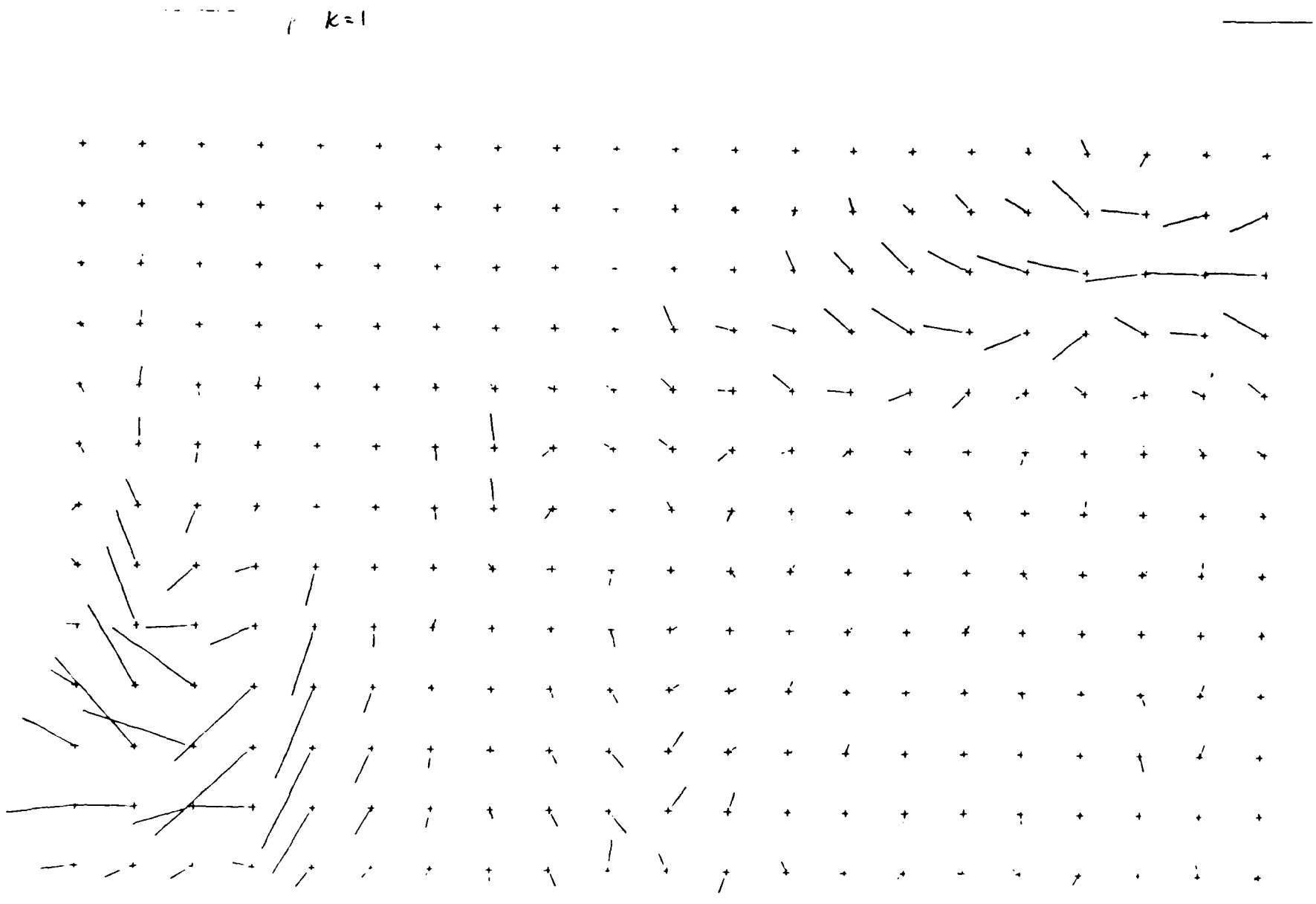

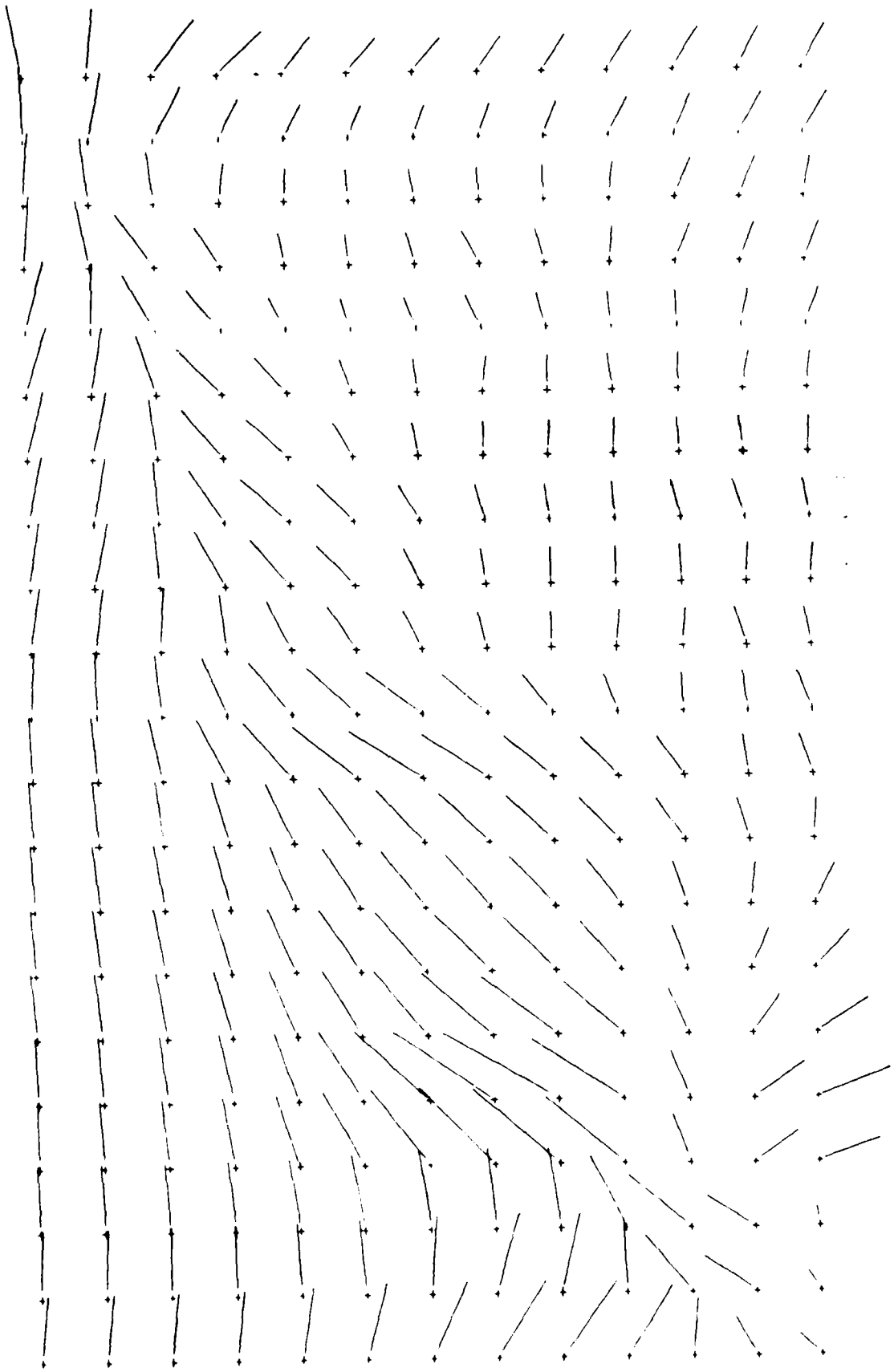
K=2

K=3

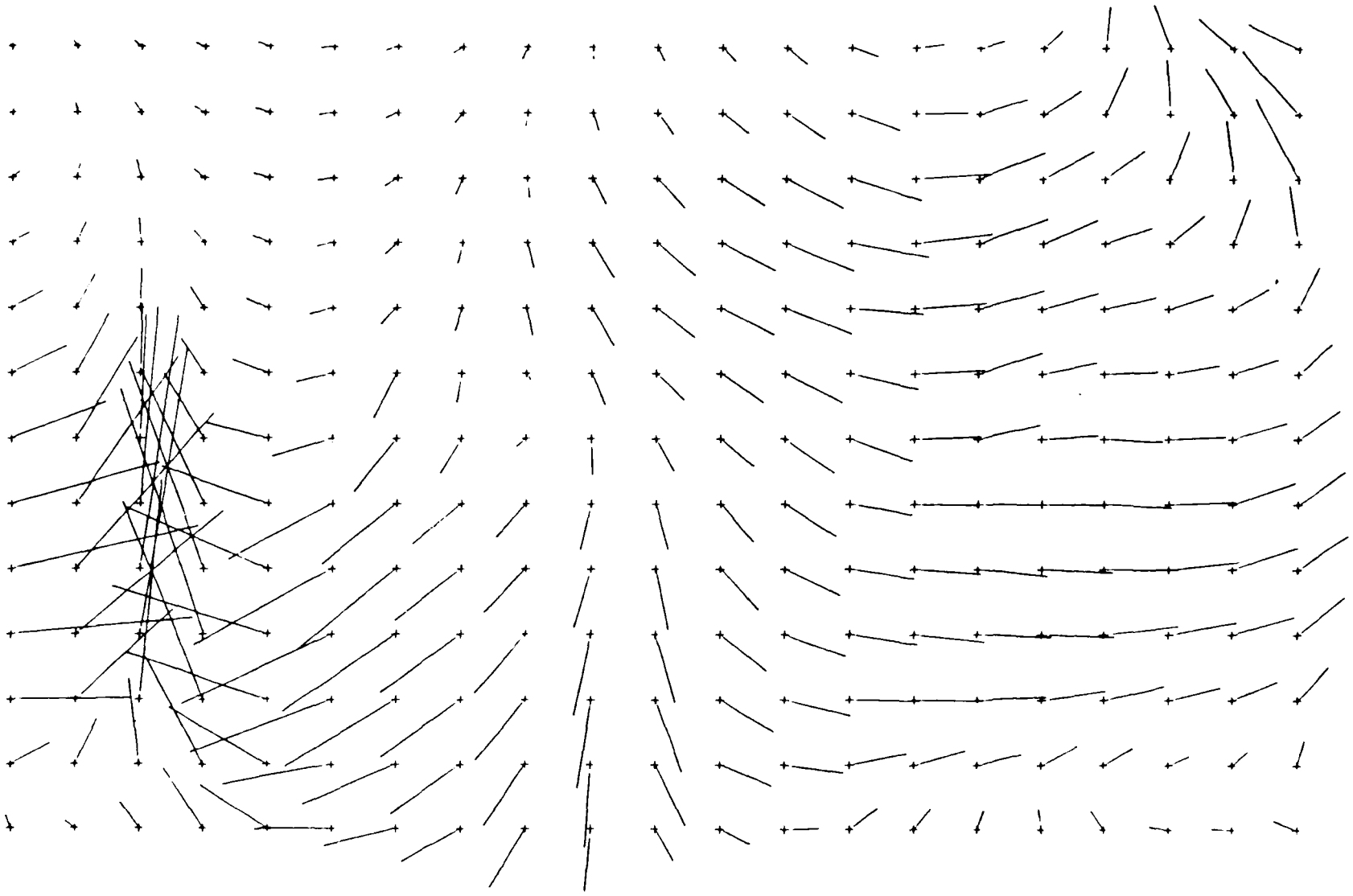

F.C. 17

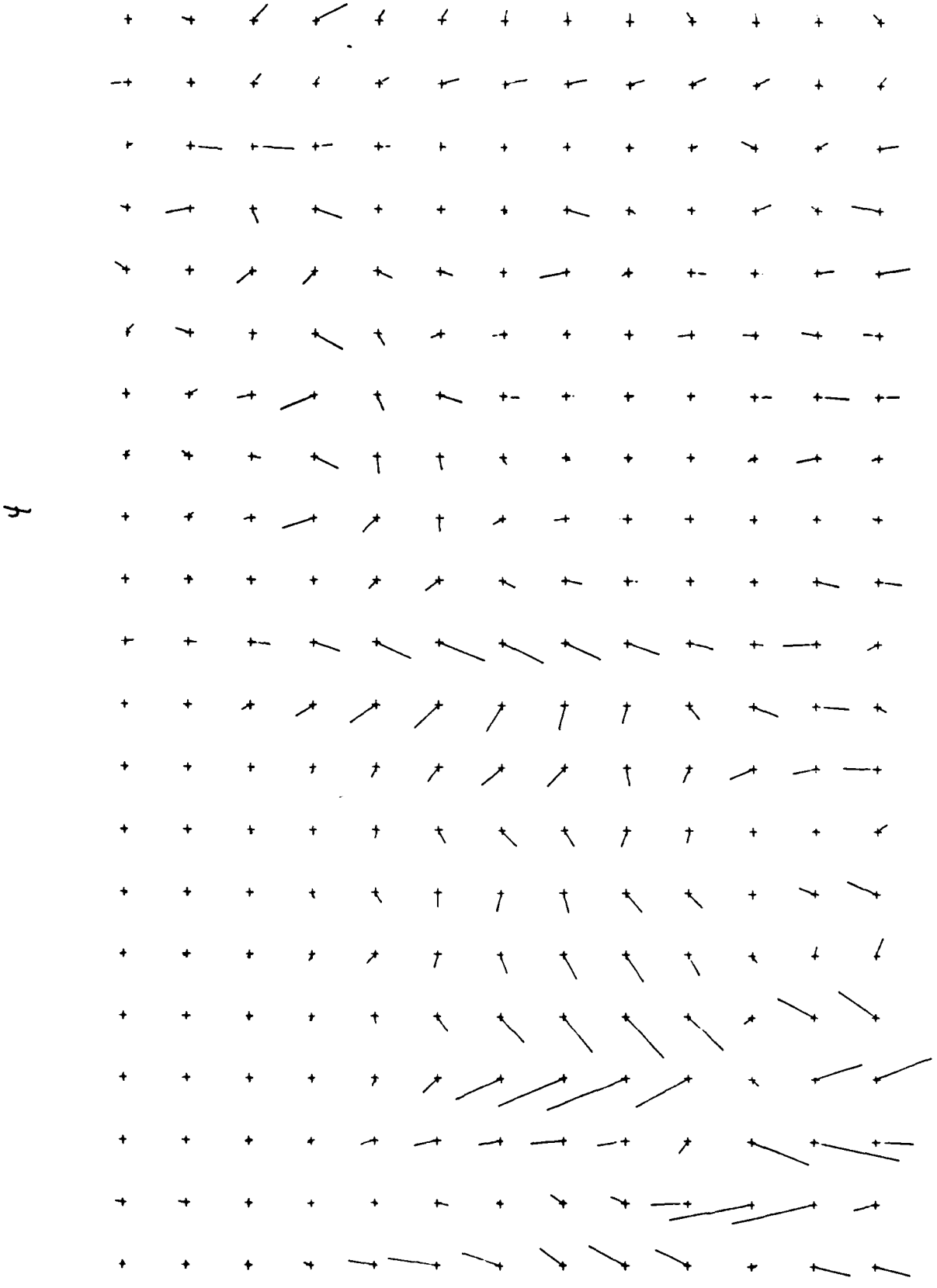

Fig 18

5

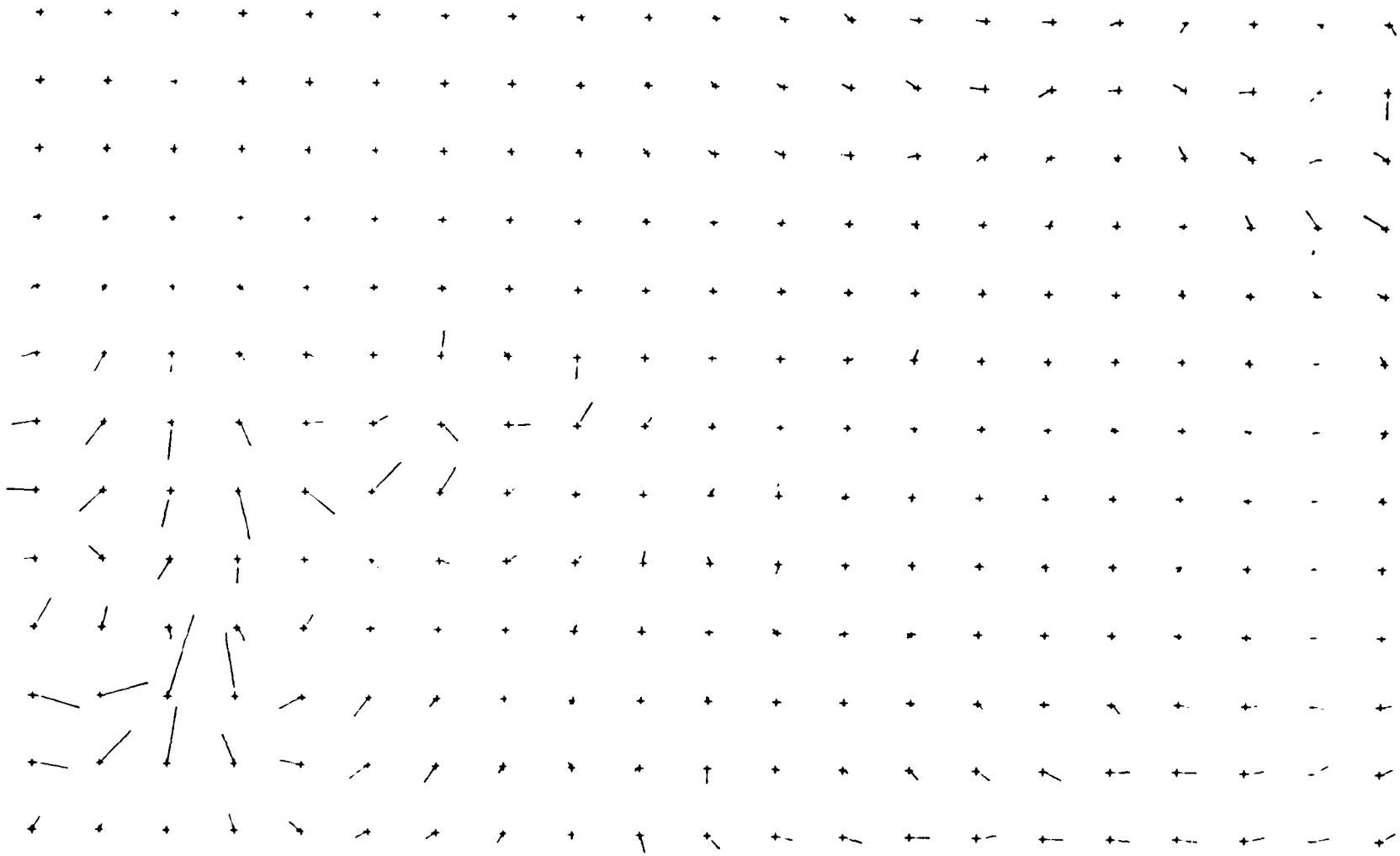

Fig 19

6

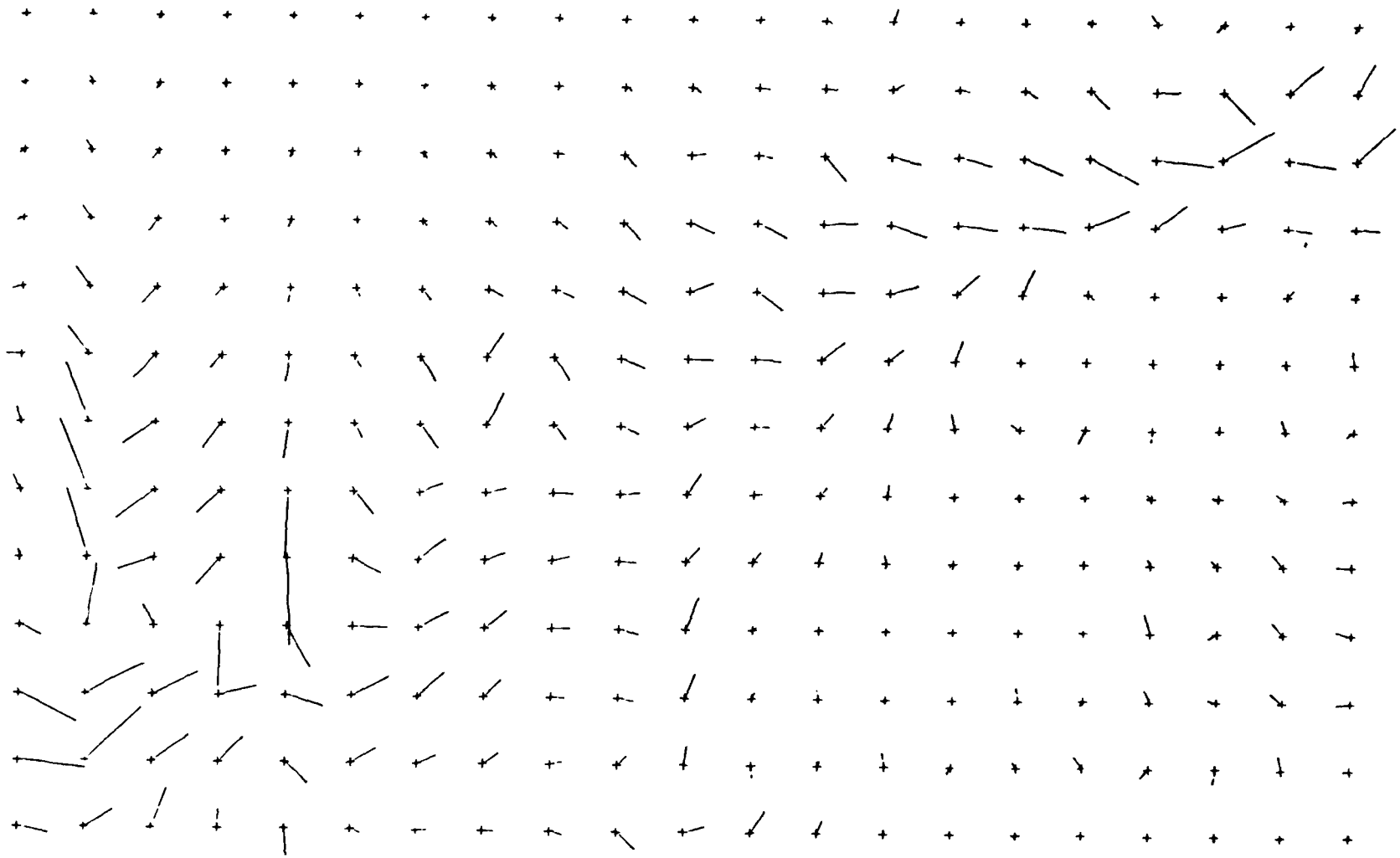

POTENTIAL APPLICATIONS OF FORCED UNSTEADY FLOWS*

Hermann Viets** and G. Michael Palmer***
West Virginia University
Morgantown, West Virginia 26506

Richard J. Bethke***
Wright State University
Dayton, Ohio 45435

Abstract

Forced unsteady flows are examined from the point of view of potential application of new devices which are made possible by the improved understanding of these flows. In particular, flows are examined which require no external driver but obtain their energy from the free-stream velocity. Other flows require no moving parts at all to generate the unsteadiness.

Introduction

Unsteady separated flows may appear as a consequence of the motion of the surface of the body or as a result of the unsteadiness in the flow over that surface. In many cases, when confronted by such flows, the objective is to eliminate or at least control the separation.

The current research program has taken a somewhat different perspective. The objective of the program is to examine the dynamics of flows which are forced to become unsteady and to specifically consider the possibilities for the application of such flows as well as determining their basic structure. In addition to the question of identifying devices which can drive a flow unsteady in a suitable way, it is necessary to determine the composition and dynamics of the large scale structures created in the periodic flow. The latter point has led to techniques which have some utility in determining the vortex structure of quasi-steady three dimensional flows.

When considering possible techniques to produce an unsteady periodic flow from a nominally steady flow, two basic requirements are apparent:

a. The device must be mechanically simple and easy to build;
b. If possible, the device should not require external power to drive it.

Past Efforts[1-7]

Under the present research program, two devices have been employed to generate the time dependence. The first is a series of purely fluidically controlled jet nozzles which satisfies both of the requirements cited above. Such a nozzle produces a jet which oscillates from side to side and results in large scale structures (shown in the flow visualization results of Figure 1) which have an important effect on the flowfield. Although these nozzles can be employed to control boundary layers, most of the effort has been applied to free jets. The jet is controlled by the fluidic feedback system wrapped around the body of the jet nozzle in Figure 2. An alternate version employing a different fluidic feedback has been found to be capable of producing an unsteady jet even if the phase of the jet flow is different from that of the surroundings.

Figure 1. Smoke flow visualization of a fluidically oscillating jet.

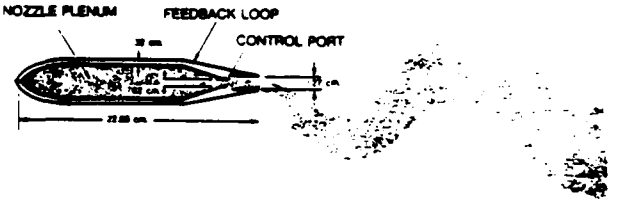

Figure 2. Schematic of the fluidically oscillating jet nozzle.

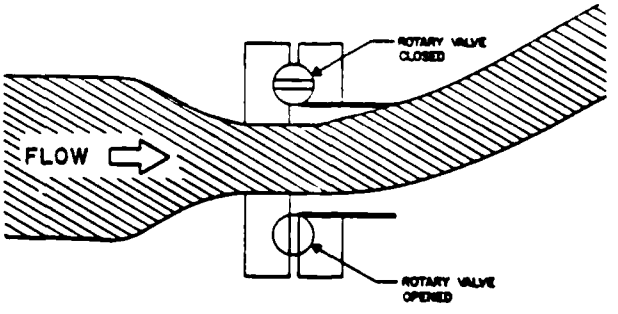

Figure 3. Schematic of the rotary valve nozzle.

* Supported by AFOSR Grant #82-0291, monitored by Capt. (Dr.) Michael S. Francis.
** Professor and Associate Dean; Presently Professor and Dean, College of Engineering, University of Rhode Island, Kingston, Rhode Island, 02881.
*** Associate Professor

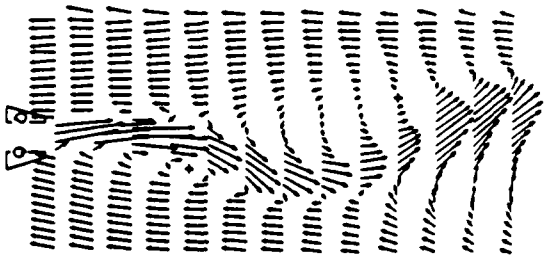

Figure 7. Rotor jet flowfield seen in a moving coordinate system.

Another problem of current interest is the application of the rotor vortex generator to reduce the drag of a bluff body vehicle. An example is a van in which the objective is to reduce the drag but to affect the volume of the van in a minimal way. Thus, simply streamlining the van has severe limitations. The method proposed is to employ the rotor to enable the flow to turn through a larger angle and thus only require a small loss of van volume due to eliminating the rear corner as shown in Figure 8. In this figure, the transformation to a coordinate frame structure dominates the flow and should lead to a drag reduction since it substantially reduces the size of the wake behind the vehicle.

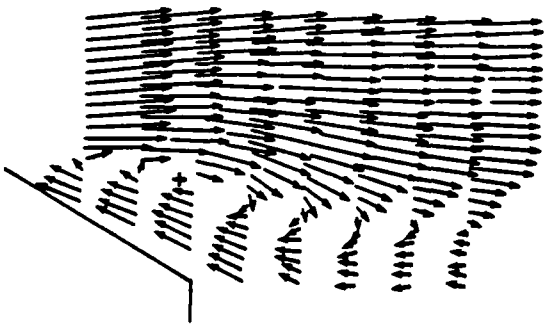

Figure 8. Flowfield produced by the rotor when applied to the wake of a van.

A third area of current interest is the dynamics of an initially rectilinear vortex structure near a wall generated by the rotor device shown in Figure 4. A schematic of the dynamics which such structure undergoes is shown in Figure 9. From the point of view of application, such a flow condition can arise behind very rapidly changed aerodynamic control surfaces. The data acquisition system described in the following section has been developed specifically for this investigation and some typical results will be shown in that section. The results with and without a shear flow profile near the wall are discussed in References 12 and 10 respectively.

Instrumentation and Data Acquisition for Forced Unsteady Flows

The instrumentations system has been designed to measure the instantaneous velocities of the convected coherent flow structures induced by the rotor motion as shown in Figure 4. The velocity (two components) is measured by an "x-wire," hot-wire anemometer and recorded by a microcomputer through an analog to digital converter. The probe positioning has been automated in one direction and is driven by the microcomputer.

The velocity of the air at any given point in the flowfield is continuously measured by the hot-wire probe. Since the structure of the flowfield generated by the rotor of Figure 4 is coherent and synchronously varying with respect to the position of the rotor upstream, the velocity is sampled with respect to the position of the rotor. Thus a complete "time picture" of the structure is obtained as it passes the probe. In addition, the coherency of the flow structures allows the signals from several successive rotations to be averaged to improve the signal to noise ratio and reduce the effects of turbulence on the measurements. The signals from the hot wire are processed and recorded by the microcomputer through an analog to digital converter.

The shaft of the rotor in Figure 4 has been fitted with a light chopper disk of two tracks. One track has a single hole used to indicate the start of the rotor orbit and the second track has thirty-six equally spaced holes (every 10°) used to indicate the position of the rotor in its orbit. These two tracks are "read" by light emitting diodes (LED), photo transistor pickups. The resulting signals are passed through an interface which provides signal conditioning to prepare the signals for the microcomputer.

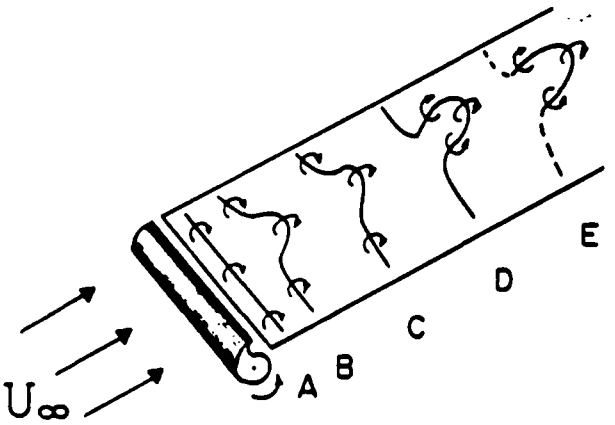

Figure 9. Schematic of the deformation of an initially rectilinear vortex.

The position of the hot-wire probe in the flowfield is partially computer controlled. The streamwise and sidewise positions of the probe are manually set while the height of the probe from the tunnel floor is computer controlled. The probe is driven up or down by a DC motor attached to a lead screw with a 24 turn-per-inch pitch. The bottom end of the lead screw is fitted with a light chopper disk with two holes. The holes are read by a LED-phototransistor pickup. The bottom end of the travel of the probe is detected by another LED-phototransistor pickup connected to a spring-loaded probe placed downstream of the hot-wire probe. The signals from the photo pickups are passed through the interface electronics to the microcomputer.

The hot-wire probe is positioned in the flow by first driving the probe to bottom and then bringing it up while counting the turns of the lead

The startup operation of the unpowered rotor device is as follows: Even if the rotor is well balanced and relatively free to turn (i.e. low frictional resistance), at low freestream velocities the rotor remains in a static orientation. As the freestream velocity is increased, the rotor assumes the position shown in Figure 11b with the cusp shape directly above the shaft. A further increase in the freestream velocity results in an oscillation or rocking of the rotor about this position. The amplitude of the oscillations increase with freestream velocity until the rotor begins to turn in the counterclockwise direction. The rotor was never observed to turn in the clockwise direction.

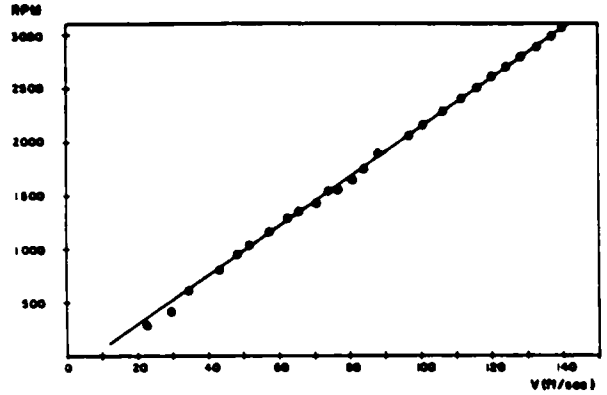

Figure 12a. Self driven rotor speed as a function of freestream velocity.

The particular rotor discussed in Reference 10 has been examined in detail to determine the relationship between the freestream velocity and rotational speed it produces. The results, shown in Figure 12a, are well represented by a linear dependence. This result is emphasized by the nondimensional results of Figure 12b where the rotational speed is reduced by V/H; the freestream velocity/exposed rotor height. Except for low freestream velocities (where both the velocities and the rotational speeds are less accurate), the reduced rotational speed is nearly constant.

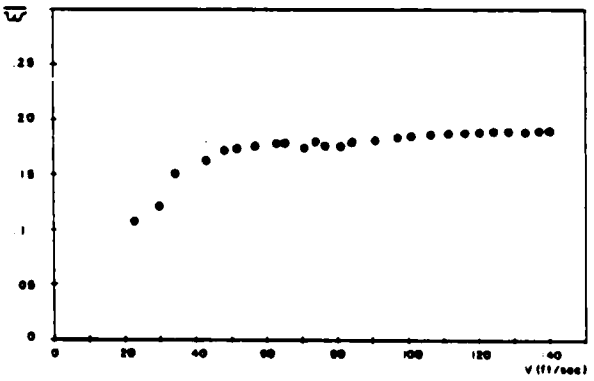

Figure 12b. Self driven rotor speed nondimensionalized with V H; freestream velocity/extended rotor height.

It should be emphasized that the results of Figures 12a and b are singular results for this particular rotor shape and for the frictional resistance of this bearing configuration. A change in the rotor shape or the frictional resistance would change the value of the curve but is not expected to affect the functional dependence.

From the point of view of potential application, the fact that the rotor can be employed without the need for an external driver is significant. It will allow more widespread use of the concept behind the device, namely the potential use of unsteady flows to achieve results superior to those found with nominally steady flows. All of the rotor based devices discussed in the preceding sections will be positively affected, from the point of view of application, by the possibility of self induced rotation.

Other Potential Applications

A wide range of potential applications exists for unsteady flow devices. Since an external driver is unnecessary to power the rotor vortex generator, the potential applications for this particular technique have improved. The following examples are all related to flow control near a solid wall and are not meant to be at all inclusive. Many other embodiments of these concepts will appear in the future.

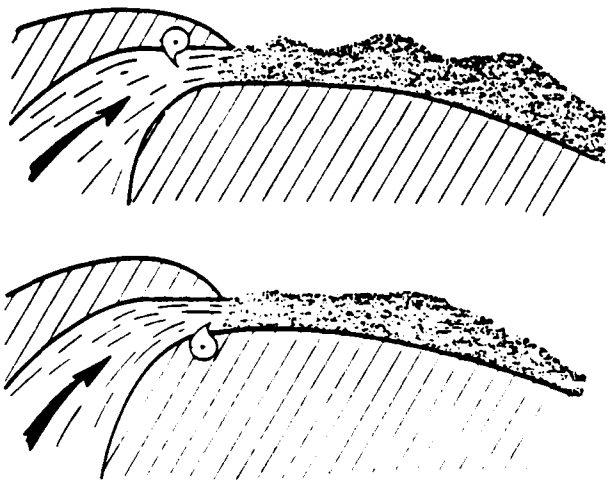

Figure 13. Two schematic embodiments of the rotor applied to a wall jet.

For the rotor concept, a wall jet version of the device is shown in Figures 13a and b where the rotor has been placed on opposite sides of a wall jet exit. In either case, the large scale vortices produced in the jet will allow the flow to remain attached to the wall in situations where it otherwise may separate. Of course, the rotor could be applied on both sides of the jet simultaneously, but it is likely that this will be unnecessary to achieve the desired structure.

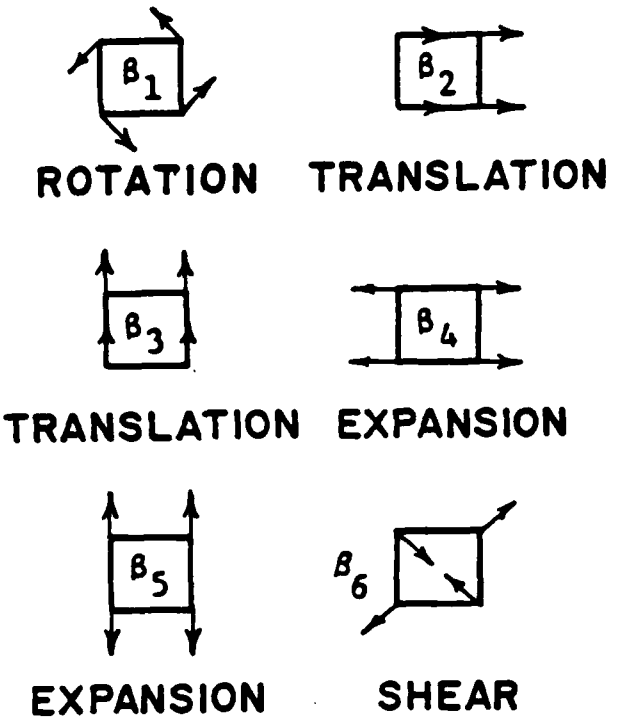

Figure 17. Orthogonal descriptors employed in the vortex identification analysis.

Figure 18. Flowfield pattern produced by the rotational descriptor.

Acknowledgement

Many thanks are due to Mont Ball and Lee Metheny for their construction of the experimental apparatus and to Frank Loth and Chris Mazur for gathering some of the data presented.

References

1. Viets, H., "Coherent Structures in Time Dependent Shear Flows", NATO AGARD [illegible] Sept. 1979.

2. Viets, H., "Unsteady Ejectors", [illegible] CP-308, Nov. 1981.

3. Viets, H., Ball, M. and Piatt, M., [illegible] in a Subscale Pilot Jet Tunnel", [illegible] Vol. 9, No. 5, 1981, pp. 820-822.

4. Viets, H., Piatt, M. and Ball, M., "Unsteady Wing Boundary Layer Energization", AIAA Paper No. 79-1631, Aug. 1979,

5. Viets, H., Piatt, M., and Ball, M., "Boundary Layer Control by Unsteady Vortex Generation", Wind Eng. and Ind. Aero., Vol. 7, 1981, pp. 135-144.

6. Viets, H. and Piatt, M., "Induced Unsteady Flow in a Dump Combustor", AIAA Progress in Astro. and Aero., Vol. 76, 1981, pp. 611-624.

7. Viets, H., Ball, M. and Bougine D., "Performance of Forced Unsteady Diffusers" - AIAA Paper No. 0154, Aerospace Sciences Meeting, St. Louis, Mo., Jan. 1981.

8. Viets, H. and Smith, J., "The Rotor Jet", in preparation.

9. Viets, H., Catalano, G. and Bougine D., "Drag Reduction by Means of Vortex Generation", in preparation.

10. Viets, H., Bethke, R.J. and Bougine, D., "Three Dimensional Vortex Dynamics Near a Wall" Fourth International Symposium on Turbulent Shear Flows, Karlsruhe, Germany, Sept. 1983.

11. Bethke, R.J. and Viets, H., "Orthogonal Decomposition Techniques to Identify Convected Flow Structures", AIAA Paper 83-0048, 1983.

12. Viets, H.; Palmer, G. M.; Loth, F.; C. Mazur, and Bethke, R. J., "Vortex Dynamic in a Shear Layer Near a Wall", in preparation.

13. Bethke, R.J. and Viets, H., "Improved Three Dimensional Analysis of Vortex Identification", in preparation.

END

5-87

DTIC